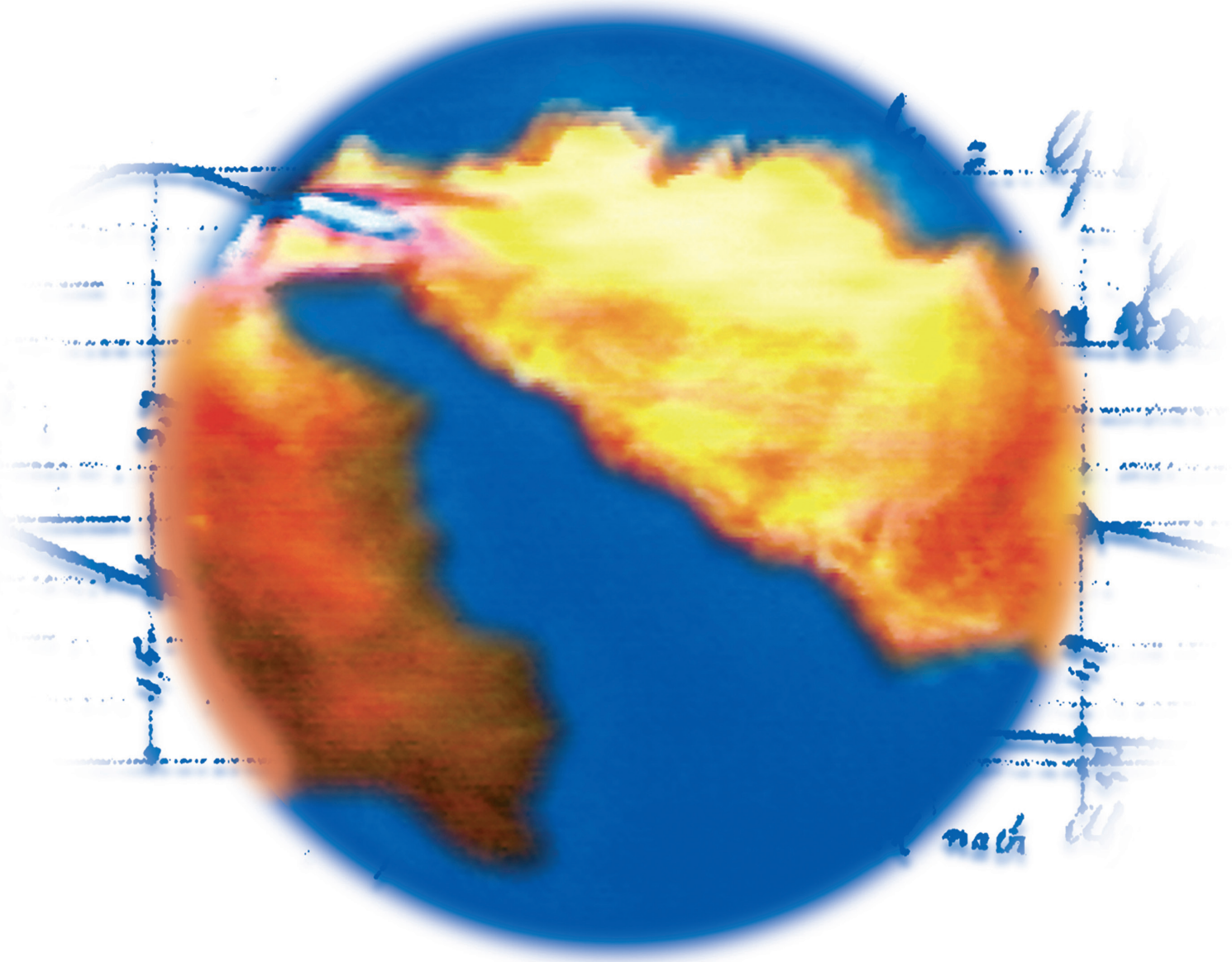

Volumenaufgelöste Geschwindigkeits- und Spraymessungen für motorische Anwendungen

Volume-resolved gas velocity and spray measurements in engine applications

Dr. Hao Chen, Prof. Dr. rer. nat. habil. Volker Sick
The University of Michigan, Ann Arbor, USA

Abstract

The ability to visualize in-cylinder phenomena in a three-dimensional (3D) manner is critical to further understand the complex physical and chemical processes within internal-combustion (IC) engines. Recently, plenoptic imaging techniques have been introduced to engine studies because they enable 3D measurements using a promising and simple single-camera setup. The fundamental concept is to record both the origin and direction of each light ray into a single light-field image by inserting a micro-lens array in front of the photosensor. Therefore, a single image contains enough information to reconstruct the 3D volume. In this study, we present the implementation of a plenoptic technique that allows 3D measurements of fuel-spray structure, as well as three-dimensional, three-component (3D3C) particle tracking velocimetry (PTV) of engine in-cylinder air flow.

Flow-spray interactions and the impact on the 3D geometry of fuel sprays were investigated with single-shot plenoptic imaging. Volume-illuminated fuel sprays from a multi-hole injector were examined in an optically accessible four-valve gasoline direct-injection engine. The impact of air flows during the intake and compression strokes on the shape of the fuel plumes could readily be observed for individual sprays without averaging.

The air flow was measured in a free jet flow and a steady-state engine flow bench employing a 3D3C PTV algorithm that analyzed volume-resolved images taken with a plenoptic camera. Silicone seed oil droplets were added to the air flows and were illuminated by the volume-expanded beam of a double-pulsed laser. Mie scattering from the droplets was recorded by the plenoptic camera, which was operated in double-frame mode. Results from the 3D3C PTV measurements were compared to two-dimensional (2D) planar particle-image velocimetry (PIV) and demonstrate the capability of the 3D velocimetry approach, presently delivering averaged flow fields.

1. Introduction

The in-cylinder fuel-air mixing, ignition and combustion processes determine not only the efficiency of IC engines, but also the harmful emissions that after-treatment systems have to manage. For instance, stratified-charge spark-ignition direct-injection (SIDI) engines, which are capable of significantly improving fuel efficiency, require careful tailoring of the fuel-air-residual gas mixture to ensure reliable ignition across a wide range of engine speeds and loads [1 – 4]. It is therefore vital to have an insightful understanding of in-cylinder processes in order to design and optimize IC engines.

Optical diagnostics have been widely utilized to visualize the complex physical and chemical processes in the combustion chamber [5-8]. Rapidly developing techniques allow measurement of fuel concentration [9], temperature distribution [10], air flow [11], soot concentration [12, 13], equivalence ratio, and burned-gas temperature [14, 15] with high temporal- and spatial resolutions. However, most of these techniques are either planar (2D), line-of-sight measurements or utilize averaging techniques to construct 3D images [16].

It has been demonstrated that there are strong cycle-to-cycle variations of the fuel spray [17], in-cylinder air flow [18, 19], ignition [20, 21] and combustion [2]. Instantaneous 3D measurements that capture these turbulent processes would provide substantial benefits over the established 2D techniques. The out-of-plane motion and gradients that typically occur within the cylinder can never be fully captured by 2D methods. Additionally, the cycle-to-cycle variations limit the application of quasi-3D techniques that involve averaging. Even rapid-scanning techniques [22-25] are barely fast enough to resolve the time scales present in IC engines.

Therefore, there is an urgent need to develop techniques that enable instantaneous 3D measurement for engine research. Han et al. [26] investigated the flame spread for an SIDI engine by a 3D visualization system using three fiber-optic photomultiplier cameras. Peterson et al. [27] presented a time-resolved multi-planar laser diagnostic technique, in which five high-speed cameras were utilized, to track the 3D motion of the early flame front in a spark-ignition engine. Baum et al. [28] demonstrated 3D velocity measurement within a $47 \times 35 \times 4 - mm^3$ volume in a motored engine by tomographic PIV. However, such measurements are always hindered by the expense of multiple cameras as well as limited optical access to the engine cylinder.

In this context, plenoptic imaging is finding its way into engine research. Plenoptic, or light-field, imaging was proposed by Lippmann [29] over a century ago. While research setups for plenoptic imaging were developed and used early as 1992 [30, 31], commercially available cameras (e. g., Lytro, Raytrix) only recently entered the market for consumer and research applications. The fundamental concept of a plenoptic camera is achieved by adding a micro-lens array directly in front of the camera sensor. Each micro-lens then acts as a camera objective to collect light from a subsection of the object from a unique perspective. In this manner, a single camera records enough information for 3D reconstruction. Advances in computational power have enabled the plenoptic camera to become a viable tool for research applications [32 – 34], because substantial processing is needed to convert raw plenoptic images into 3D representations.

Greene and Sick [35] showed the application of plenoptic imaging to 3D measurements of flame chemiluminescence and laser-induced fluorescence of nitrogen jets seeded with acetone. This work also identified the need to improve image reconstruction for translucent objects, where the path of light from the object to the camera is not constrained by an opaque surface that provides high contrast. For non-opaque objects, multiple reconstruction solutions exist, which may lead to artifacts and errors in the reconstructed images.

To overcome these issues, model-based reconstruction techniques are currently in development and are being explored to better address imaging of translucent systems [36]. For optically dense objects, such as fuel sprays early in their development, our previous studies [37, 38] have demonstrated accurate 3D evaluation capabilities of plenoptic imaging systems. Additionally, plenoptic imaging has the potential to extend the well established planar PIV technique towards single-camera three-dimensional, three-component (3D3C) measurement [39 – 42].

This paper presents applications of plenoptic imaging that show how the 3D geometry of fuel sprays is affected by interaction between the spray and the in-cylinder gas flow under both homogeneous-charge (fuel injection during intake stroke) and stratified-charge (fuel injection late in compression stroke) modes in a motored SIDI optical engine. Moreover, the capability of 3D3C velocity measurements with a single-camera plenoptic system is demonstrated in a low-turbulence jet flow and steady-state engine flow bench. This demonstration shows the opportunity to enhance measurement capabilities in widely used steady-flow benches and eventually will allow such 3D3C PTV measurements in engines.

2. Experimental Setups

2.1 Plenoptic-Camera Setup

A 29-megapixel color plenoptic camera (R29, Raytrix GmbH) was used in this study. However, due to the reconstruction procedures necessary to obtain 3D images, the effective resolution is reduced to 7 megapixels [43]. Both micro-lens array (MLA) calibration and spatial calibration must be conducted when either the focus setting or the

aperture is changed. The MLA calibration fits a calibration grid with the micro-lens images using homogeneous illumination. Then, spatial calibration determines the relationship between the virtual depth and the physical depth by capturing a series of calibration target images with different orientations. The calibration target is placed at an oblique angle to the camera axis with the aim of covering the entire depth-of-field. After completing these two steps, the camera is fully calibrated for a given imaging setting. For the flow measurements present here, the depth-of-field is approximately 25 mm with a depth resolution of 90-350 µm, depending on the distance to the camera. For the fuel-spray imaging setup, the depth-of-field is about 40 mm with a depth esolution of 150 – 650 µm.

To assess the quality of the depth calculation of the plenoptic imaging system, a simple setup was built as shown in Figure 1. A known-dimension dot array was placed at 60° to the surface of the table. The tilted dot array creates a depth range that is similar to that of the PTV flow experiment discussed below. Each dot (standing in for a PTV particle, though considerably larger) is imaged by several micro-lenses. The images are then reconstructed in post-processing to provide the dot's three spatial coordinates. Figure 2 depicts the depth evaluation result, in which grayscale is utilized to represent the depth. The depth error is within 300 µm for the whole depth range.

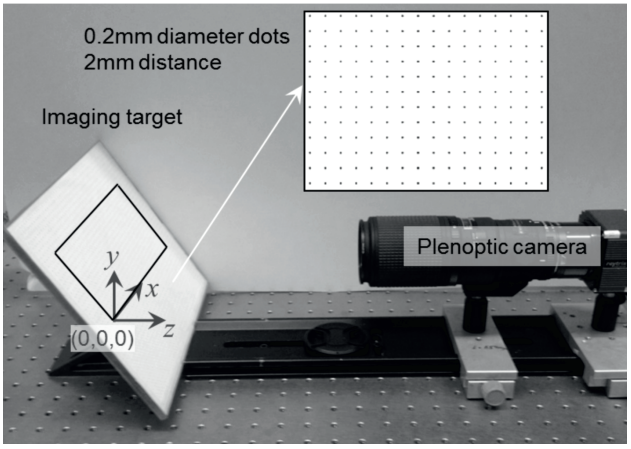

Figure 1:
Setup to assess the depth evaluation produced by the plenoptic imaging system. The dot-array target is positioned at an angle of 60° with respect to the table surface.

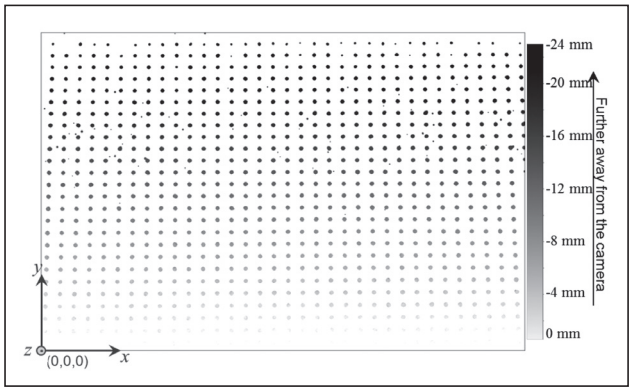

Figure 2:
Grayscale depth map evaluated by the plenoptic imaging system.

2.2 Optical-Engine Setup

The fuel-spray study was conducted in a SIDI single-cylinder, four-stroke, four-valve optical engine. As shown in Figure 3, the engine has a pent-roof combustion chamber, with an eight-hole injector tilted by 8° with respect to the cylinder axis. The injector generates a symmetric pattern of eight plumes with a nominal spray angle of 90° and is oriented so that two fuel plumes straddle the spark plug. A quartz cylinder, two head windows, and piston windows offer extensive optical access into the combustion chamber. More details regarding the engine can be found in a previous study [44].

As depicted in Figure 3a, a 527-nm Nd-YLF laser (Quantronix Darwin Duo) set to pulse energies of 0.2 mJ was used as the illumination source. The laser beam was expanded to illuminate the entire fuel spray, and the camera then recorded the fuel spray through the piston window. One example of the recorded raw plenoptic spray image is shown in Figure 3b. The 3D reconstruction of the spray image was performed in the RxLive (Raytrix GmbH) software.

Spray images under static (engine not running), and two non-fired motored conditions were recorded to highlight the impact of in-cylinder flows on the spray evolution. The two motored conditions differed by start-of-injection (SOI) timing; both 300° before top dead center (BTDC) compression, as in homogeneous-charge SIDI combustion, and 35° BTDC, as in stratified-charge SIDI combustion, were used. The engine was motored at 1300 rpm with 95-kPa intake-manifold absolute air pressure. 10 mg of isooctane was injected with a pressure of 12 MPa during each cycle.

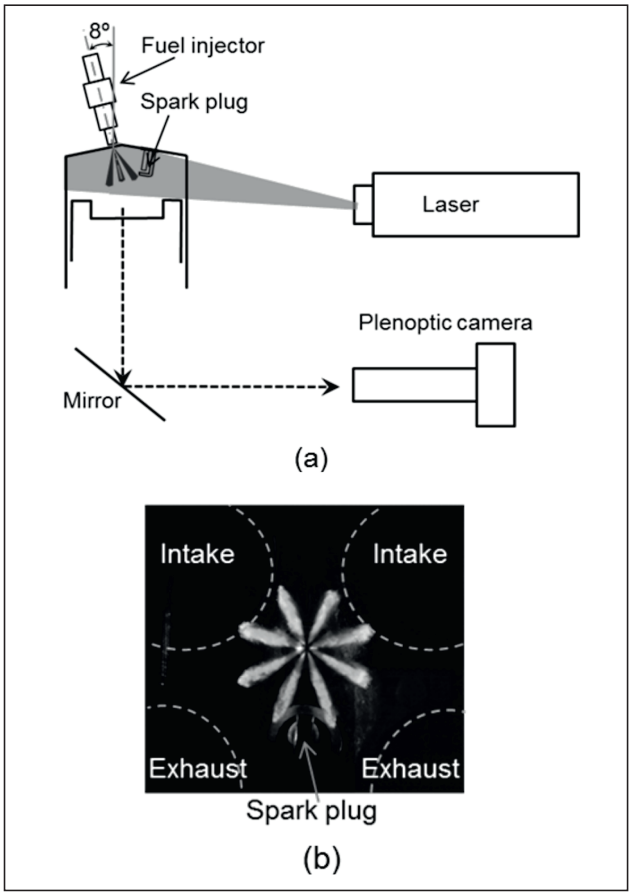

Figure 3:
(a) Experimental setup for 3D spray imaging in the optical engine;
(b) raw plenoptic spray image example as viewed from below
(indicated by the dashed line in Figure 3a) with valve and spark-plug positions indicated.

2.3 Steady-Flow Setups

Prior to measuring 3D velocity fields in the complex engine environment, the plenoptic PTV technique was characterized for simpler flows, such as low-turbulence jet flow, and then on a steady-state engine flow bench. Proper characterization also includes benchmarking the plenoptic technique against the established 2D PIV technique. Future work then includes measuring instantaneous 3D velocity fields in operating optical engines with benchmark comparison to existing comprehensive 2D PIV measurements [45].

Figure 4 displays the experimental setup for the jet-flow measurement. To ensure the air flow (seeded with silicone oil droplets, about 1 µm diameter) is fully developed, a long straight circular pipe (L/D = 41, D = 24 mm) is used. The Reynolds number of the flow is approximately 3600. The double-frame plenoptic PTV system employs a dual-cavity PIV laser (Litron Nano T 120-15) with beams that are expanded to volumetrically illuminate the droplets exiting the pipe. The plenoptic camera captures image pairs with a time delay of 50 µs, selected to achieve the best particle displacements between images for the given flow settings. The plenoptic camera is tilted at an angle of 60 degrees with respect to the pipe axis. Thereby, the ability to capture the velocity along the depth direction can be evaluated.

The steady-state flow characterization of a cylinder head is a procedure that is widely utilized to assist and assess the design of the intake ports and the combustion chamber geometry [46, 47]. Adding 3D PTV measurement capability to a steady-state engine flow bench could provide additional valuable information compared to the conventional intrusive swirl and tumble number measurements. Figure 5 shows the engine flow-bench model built for this study. The geometry of the intake runner and the engine head are identical to the optical engine shown in Figure 3. The air is seeded with silicone oil droplets and flows through the intake plenum, intake runner, intake ports, and intake valves, before finally entering the quartz engine cylinder. The measurement volume is illuminated by the above-mentioned double-pulsed Litron PIV laser to create Mie-scattering signals that are recorded by the plenoptic camera running in double-frame mode with a time delay of 50 µs between the two frames.

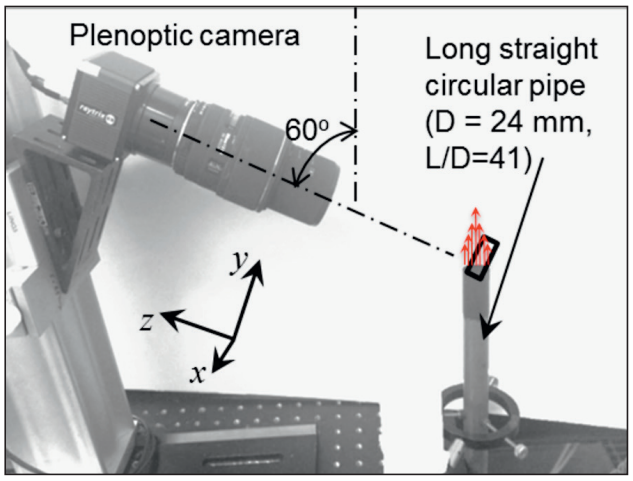

Figure 4:
Experimental setup for bench-top jet-flow measurement. Reynolds number ≅ 3,600.

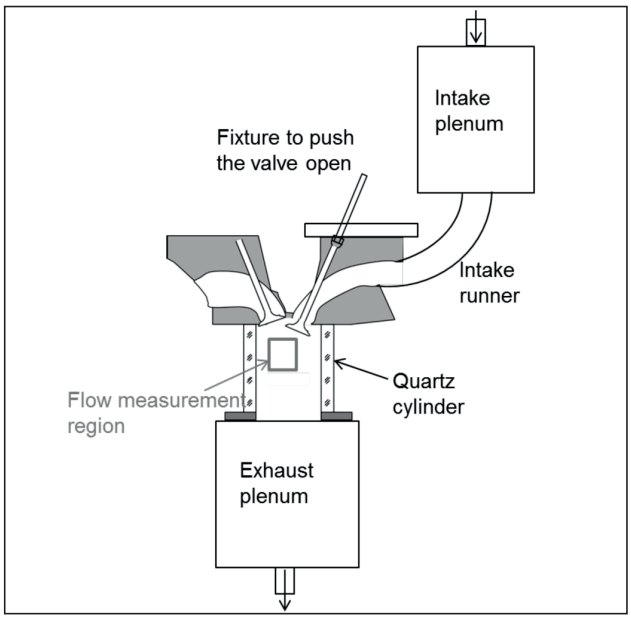

Figure 5:
Steady flow bench setup with optically accessible SIDI geometry.

3. Image Processing

The image processing procedure for the spray study is detailed in a previous publication [38] and only briefly summarized here. The RxLive software (Raytrix GmbH) was used for the spray-depth evaluation. The raw plenoptic spray images were preprocessed to enhance their contrast. The increased contrast improves the accuracy of the 3D reconstruction process. The 3D reconstruction resulted in thousands of data points representing the location of the liquid spray in all three dimensions. Finally, a depth-fill interpolation was applied to generate a smooth "depth map."

This section emphasizes the procedure for the PTV processing. The raw particle images were processed using the RxFlow software (Raytrix GmbH). The particle location in all three dimensions was determined quantitatively using the calibration procedure described in Section 2.1. Then, the displacement of the particles between the double-frame images was computed by a particle-tracking analysis. This analysis yielded individual 3D particle positions and corresponding displacements, which are associated with the local velocity. The subsequent post-processing interpolated the velocities onto a uniform grid. In order to keep a low probability of false particle matching due ambiguities of distinguishing particles that are in close proximity to each other, a relatively low seeding density (0.0002 ~ 0.0003 particles per pixel) had to be utilized. As a result, the instantaneous 3D velocity fields do not have enough vectors to generate a comprehensive flow-field representation, and a sequence of double-frame images was required to produce an averaged 3D velocity field.

To quantitatively evaluate the accuracy of the 3D PTV system, a standard 2D PIV measurement was conducted separately on the jet flow. For this comparison, the plenoptic camera was set up exactly as in Figure 4. However, instead of using volumetric illumination, a 1-mm-thick laser sheet was created and passed through the jet axis. Figure 6a shows the total-focused image, which means the particle images within the whole depth-of-field were computationally refocused, just like a conventional 2D digital photo would appear. The seeding density was also increased for the 2D PIV to achieve 8 ~ 15 particles per interrogation window, as suggested by Keane and Adrian [48] and

verified experimentally by Megerle et al. [49]. For the current settings, the particles that are closer to the camera (upper part of Figure 6a) are not as focused as the particles that are further away from the camera (lower part of Figure 6a). This phenomenon is due to the reduced near-field (close to the camera) depth resolution (¼ of far field resolution) inherent in the type of plenoptic camera used for this study (one employing a micro-lens array with three types of lenses of different focal length).

Images obtained with sheet illumination were utilized for two purposes. First, accurate evaluation of the depth positions of the particles was confirmed, utilizing the known dimensions of the pipe and the camera tilting angle, as seen in Figure 6b. Second, the 2D images were processed using the well-established 2D PIV cross-correlation algorithm in the LaVision DaVis 8 software. Then, the obtained velocity in the pipe-axis direction was decomposed into the y-direction and z-direction (as indicated in Figure 4) based on the camera tilting angle. In this manner, the quality of the 3D PTV results was quantitatively assessed by comparing them to the 2D PIV results described in section 4.2.

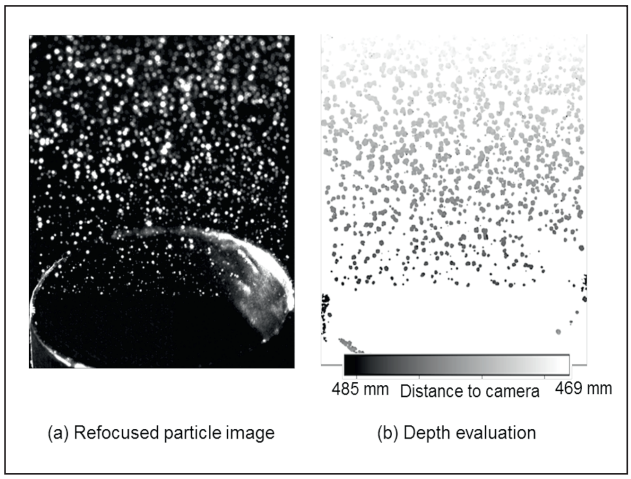

Figure 6:
Depth evaluation for the particle image.

4. Results and Discussion

4.1 3D-Spray Measurements

Figure 7 depicts the 3D fuel-spray structure – grayscale represents the third dimension of the spray – under static in-cylinder conditions (stationary piston and valves), homogeneous-charge mode (fuel injection early in the intake stroke), and stratified-charge mode (fuel injection late in the compression stroke). In Figure 7a, the apparent difference in spray penetration between spray plumes 1 and 2 relative to plumes 5 and 6 is due to the 8° angle that exists between the fuel injector and the camera's optical axis. Compared to the symmetric spray structure in static conditions, the strong intake-air motion rotates the spray and reduces the spray penetration in Figure 7b. In Figure 7c, the spray structure is minimally influenced due to the weak air flow during the compression stroke, but the increased ambient pressure and temperature lead to shorter penetration than in atmospheric conditions. A much larger set of measurements and results were presented separately [38].

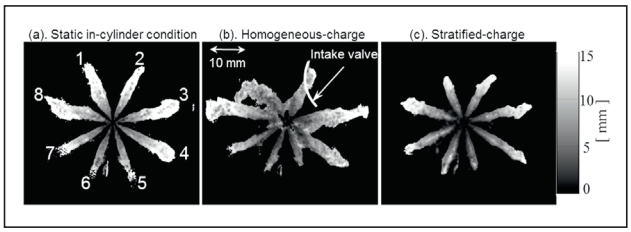

Figure 7:
3D fuel-spray structure for (a) static (quiescent) in-cylinder condition (b) homogeneous-charge operating condition, and (c) stratified-charge operating condition. (Adapted from [38], DOI: 10.1177/1468087415608741).

4.2 3D-Flow Measurements

Figure 8 shows the 3D velocity distribution in a section of the jet flow that is highlighted by the rectangle in Figure 4. The number of vectors in the instantaneous velocity field is limited by the low seeding density, therefore the 3D3C velocity distribution is computed by interpolating and averaging 200 instantaneous velocity fields. These fields are then further grouped into discrete layers for visualization purposes. Four layers normal to the camera axis at different distances from the camera in the z direction with a resolution of 4 mm in this direction are shown here.

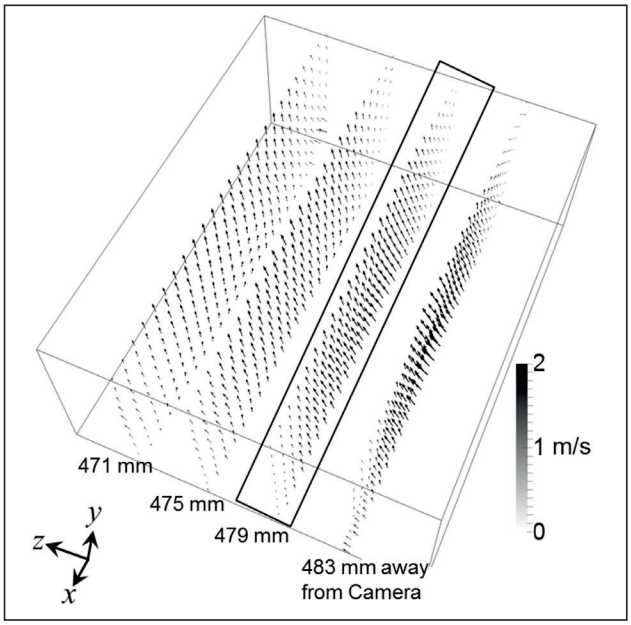

Figure 8:
3D velocity field of the jet flow. Measurement volume: 24 × 9 × 12 mm^3 for x, y, and z respectively. Spatial resolution: 1 mm for x and y directions and 2 mm for z direction, but every other vector in this direction is shown for clarity).

Figure 9 compares a slice of the 3D velocity distribution (highlighted in Figure 8) with the 2D PIV results. The illuminating light sheet for the PIV measurement was aligned vertically along the jet axis. Note that therefore, in contrast to the sample planes shown in Fig. 8, the measurement plane extracted from the volumetrically resolved measurements is parallel to the jet axis, matching the location of the PIV light sheet. Qualitatively, the velocity magnitudes and velocity fields are similar for both measurements. The velocity magnitude along one line (y = 6 mm) is quantitatively compared in Figure 10. Overall, 200 image pairs

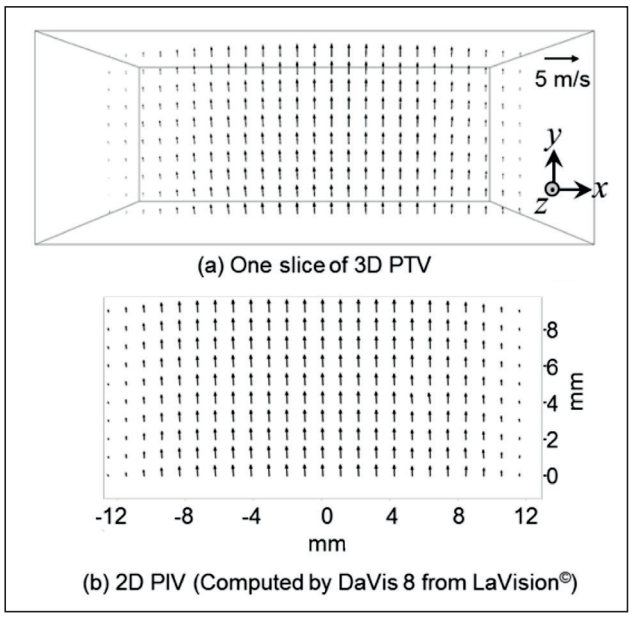

Figure 9:
Comparison between one slice of 3D PTV (from ParaView) and the standard planar PIV (from DaVis). Note that x=0 is located in the center of the jet and y = 0 is at the nozzle exit.

were computed for 2D PIV; the average and its standard deviation, shown as error bars, are included in Figure 10. The velocity along the y direction for 3D PTV agrees very well with the 2D measurement. The velocity along the z direction also agrees except between x = 8 ~ 12 mm. The cause of this discrepancy has not yet been determined.

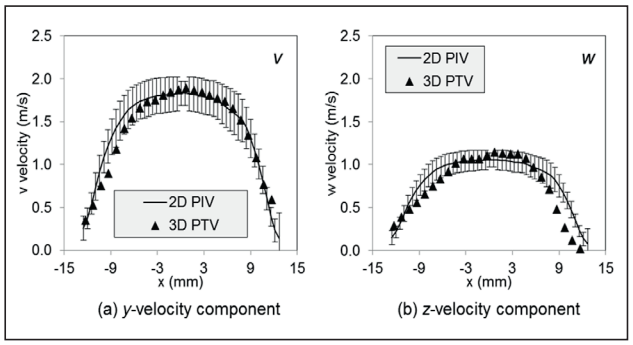

Figure 10:
Comparison between 2D and 3D measurements along line y = 6mm in the plane shown by Fig. 9.

This example showed the current status of quantitative flow measurements with the 3D3C velocity measurement in a steady flow situation. Building on this result, the averaged velocity field in the steady-state engine flow bench was then measured. Figure 11 illustrates the typical tumble flow structure, which is created by the intake valves located offset from the axis of the engine cylinder. In Figure 11, the curved arrow demonstrates this flow structure, while the rectangle highlights the region in which the 3D PTV measurement was performed. The larger field of view shows in-plane velocities, measured by 2D PIV.

The plenoptic 3D velocity field is shown in Figure 12. The measurement volume is 20 × 24 × 10 (x, y, z respectively) mm³, the resolution is 2 mm for all three dimensions. Note that this resolution is

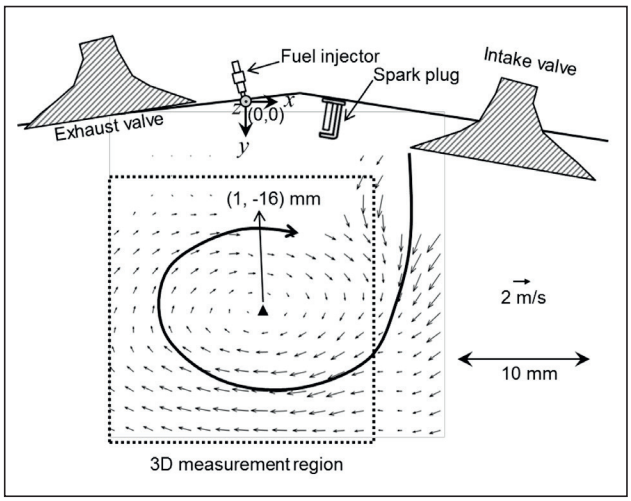

Figure 11:
Velocity distribution measured in the steady-state engine flow bench.

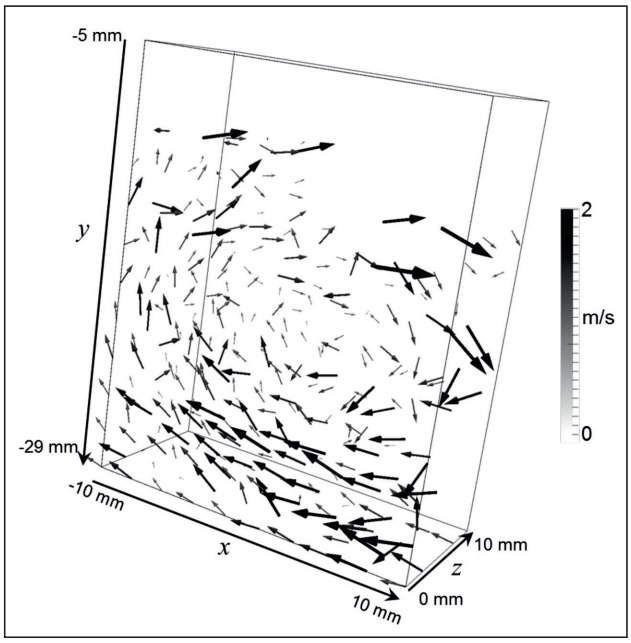

Figure 12:
3D velocity distribution computed from the 3D particle positions using RxFlow (Raytrix).

different from that of the 2D PIV processing, which is 1.5 mm. The PIV algorithm defines a fixed interrogation window, but it is difficult for the 3D PTV to reach this resolution, especially for the depth direction. Again, this 3D velocity distribution was calculated by interpolating and averaging of, in this case, 395 instantaneous velocity fields. The overall tumble structure and the location of the tumble center (as indicated by a triangle in Figure 11 and Figure 13) are reasonably well captured by the 3D PTV measurement. Moreover, the velocity gradient along the third dimension can be observed in the 2D slices shown in Figure 13. Part of a potential vortex can also be seen in Figure 13a.

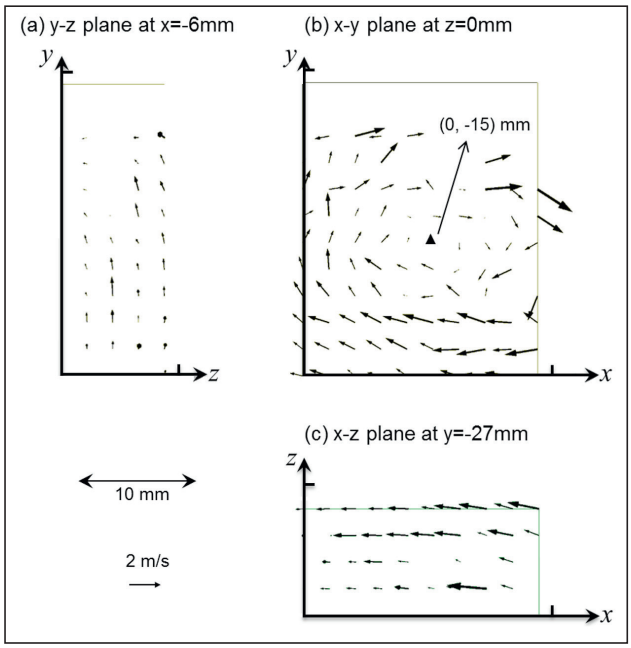

Figure 13:
2D-slices from the 3D velocity field shown in Figure 12.

5. Conclusions

A compact and promising single-camera setup that enables 3D measurements of spray geometry and velocity field was demonstrated in an optical SIDI engine, a low-turbulence jet flow, and an engine steady-flow bench. The core component for all of these measurements is a large-format plenoptic camera that enables instantaneous 3D imaging. Pulsed laser illumination provided the temporal resolution that was desired for this study.

The impact of in-cylinder flow on 3D fuel-spray structure was robustly captured with the plenoptic imaging setup. Deflections of individual fuel plumes from a multi-hole injector under different engine conditions were captured. The observations are in agreement with expectations from previous studies, but now added information is available in single-shot imaging. This single-shot capability is especially important for measurements of cycle-to-cycle variations.

Initial results to determine volume-resolved velocity fields yielded promising results. Comparison to 2D PIV subsets identified areas of necessary improvements. Examples studied include a jet flow out of a straight pipe and measurements in an engine steady-flow bench setup where the expected tumble flow could clearly be measured with the plenoptic setup.

Acknowledgements

This material is based upon work supported by the National Science Foundation under Grant No. CBET 1402707.

References

[1] B. Peterson; D. L. Reuss and V. Sick, "High-speed imaging analysis of misfires in a spray-guided direct injection engine," Proceedings of the Combustion Institute, vol. 33, pp. 3089 – 3096, 2011.

[2] B. Peterson; D. L. Reuss and V. Sick, "On ignition and flame development in a spray-guided direct-injection spark-ignition engine," Comb. and Flame, p. http://dx.doi.org/10.1016/j.combustflame.2013.08.019, 2013.

[3] H. Chen; D. Reuss and V. Sick, "Analysis of misfires in a direct injection engine using proper orthogonal decomposition," Experiments in Fluids, vol. 51, pp. 1139 – 1151, 2011.

[4] T. D. Fansler; D. L. Reuss; V. Sick and R. N. Dahms, "Invited Review: Combustion instability in spray-guided stratified-charge engines: A review," International Journal of Engine Research, vol. 16, pp. 260 – 305, 2015.

[5] V. Sick, "High Speed Imaging in Fundamental and Applied Combustion Research," Proceedings of the Combustion Institute, vol. 34, pp. 3509 – 3530, 2013.

[6] V. Sick; M. C. Drake and T. D. Fansler, "High-speed imaging for direct-injection gasoline engine research and development," Experiments in Fluids, vol. 49, pp. 937 – 947, 2010.

[7] H. Zhao, Laser Diagnostics and Optical Measurement Techniques in Internal Combustion Engines: SAE International, 2012.

[8] [G. P. Merker; C. Schwarz and R. Teichmann, Combustion Engines Development: Mixture Formation, Combustion, Emissions and Simulation: Springer Heidelberg Dordrecht London New York, 2012.

[9] J. D. Smith and V. Sick, "Quantitative, dynamic fuel distribution measurements in combustion-related devices using laser-induced fluorescence imaging of biacetyl in iso-octane," Proceedings of the Combustion Institute, vol. 31, pp. 747 – 755, 2007.

[10] M. E. Cundy; P. Trunk; A. Dreizler and V. Sick, "Gas-Phase Toluene LIF Temperature Imaging Near Surfaces at 10 kHz," Experiments in Fluids, 2011.

[11] H. Chen; M. Xu and D. Hung, "Analyzing In-cylinder Flow Evolution and Variations in a Spark-Ignition Direct-Injection Engine Using Phase-Invariant Proper Orthogonal Decomposition Technique," presented at the SAE Technical Paper 2014-01-1174, 2014.

[12] S. Hemdal; M. Andersson; P. Dahlander; R. Ochoterena and I. Denbratt, "In-cylinder soot imaging and emissions of stratified combustion in a spark-ignited spray-guided direct-injection gasoline engine," International Journal of Engine Research, vol. 12, pp. 549 – 563, December 1, 2011.

[13] B. D. Stojkovic; T. D. Fansler; M. C. Drake and V. Sick, "High-Speed Imaging of OH* and Soot Temperature and Concentration in a Stratified-Charge Direct-Injection Gasoline Engine," Proceedings of the Combustion Institute, vol. 30, pp. 2657 – 2665, 2005.

[14] M. Mosburger; V. Sick and M. C. Drake, "Quantitative high-speed burned gas temperature measurements in internal combustion engines using sodium and potassium fluorescence," Applied Physics B, vol. 110, pp. 381 – 396, 2013/03/01 2013.

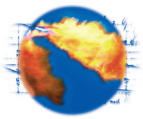

[15] M. Mosburger; V. Sick and M. C. Drake, "Quantitative high-speed imaging of burned gas temperature and equivalence ratio in internal combustion engines using alkali metal fluorescence," International Journal of Engine Research, vol. 15, pp. 282 – 297, April 1, 2014.

[16] D. Frieden and V. Sick, "Investigation of the fuel injection, mixing and combustion processes in an SIDI engine using quasi-3D LIF imaging," SAE Transactions Journal of Engines, pp. 270 – 281, 2003.

[17] H. Chen; D. S. Hung; M. Xu; H. Zhuang and J. Yang, "Proper orthogonal decomposition analysis of fuel spray structure variation in a spark-ignition direct-injection optical engine," Experiments in Fluids, vol. 55, pp. 1 – 12, 2014/03/25 2014.

[18] W. Zeng; M. Sjöberg and D. L. Reuss, "PIV examination of spray-enhanced swirl flow for combustion stabilization in a spray-guided stratified-charge direct-injection spark-ignition engine," International Journal of Engine Research, vol. 16, pp. 306 – 322, April 1, 2015.

[19] D. L. Reuss,"Cyclic Variability of Large-Scale Turbulent Structures in Directed and Undirected IC Engine Flows," SAE Technical Paper 2000-01-0246, 2000.

[20] H. Chen; M. Xu; D. L. S. Hung and H. Zhuang, "Cycle-to-cycle variation analysis of early flame propagation in engine cylinder using proper orthogonal decomposition," Experimental Thermal and Fluid Science, vol. 58, pp. 48–55, 10// 2014.

[21] D. L. S. Hung; H. Chen; M. Xu; J. Yang and H. Zhuang, „Experimental Investigation of the Variations of Early Flame Development in a Spark-Ignition Direct-Injection Optical Engine," Journal of Engineering for Gas Turbines and Power, vol. 136, pp. 101503 – 101503, 2014.

[22] J. Weinkauff; M. Greifenstein; A. Dreizler and B. Böhm, "Time resolved three-dimensional flamebase imaging of a lifted jet flame by laser scanning," Measurement Science and Technology, vol. 26, p. 105201, 2015.

[23] K. Y. Cho; A. Satija; T. L. Pourpoint; S. F. Son and R. P. Lucht, "High-repetition-rate three-dimensional OH imaging using scanned planar laser-induced fluorescence system for multiphase combustion," Applied Optics, vol. 53, pp. 316 – 326, 2014/01/20 2014.

[24] S. Johan; K. Elias; R. Mattias; A. Marcus; G. Guido and K. Kai, "Ultra-high-speed pumping of an optical parametric oscillator (OPO) for high-speed laser-induced fluorescence measurements," Measurement Science and Technology, vol. 20, p. 025306, 2009.

[25] J. Olofsson; M. Richter; M. Aldén and M. Augé, "Development of high temporally and spatially (three-dimensional) resolved formaldehyde measurements in combustion environments," Review of Scientific Instruments, vol. 77, p. 013104, 2006.

[26] K.-M. Han; A. Velji and U. Spicher, "A New Approach for Three-Dimensional High-Speed Combustion Diagnostics in Internal Combustion Engines," 2006.

[27] B. Peterson; E. Baum; B. Boehm and A. Dreizler, "Early flame propagation in a spark-ignition engine measured with quasi 4D-diagnostics," Proceedings of the Combustion Institute, vol. 35, pp. 3829–3837, 2015.

[28] E. Baum; B. Peterson; C. Surmann; D. Michaelis; B. Böhm and A. Dreizler, "Investigation of the 3D flow field in an IC engine using tomographic PIV," Proceedings of the Combustion Institute, vol. 34, pp. 2903 – 2910, // 2013.

[29] G. Lippmann, „Epreuves reversibles, photographies integrales," Comptes Rendus de l'Académie des Sciences, vol. 146, p. 446 – 551, 1908.

[30] R. Ng; M. Levoy; M. Brédif; G. Duval; M. Horowitz and P. Hanrahan, "Light Field Photography with a Hand-Held Plenoptic Camera," Stanford University Computer Science Tech Report CSTR2005.

[31] E. H. Adelson and J. Y. A. Wang, "Single lens stereo with a plenoptic camera," IEEE Transactions on Pattern Analysis and Machine Intelligence, vol. 14, pp. 99 – 106, 1992.

[32] U. Perwass, "Digital imaging system for synthesizing an image using data recorded with a plenoptic camera," European Patent EP2244484 A1, 2010.

[33] T. W. Fahringer and B. S. Thurow, "Tomographic Reconstruction of a 3-D Flow Field Using a Plenoptic Camera," in 42nd AIAA Fluid Dynamics Conference and Exhibit, New Orleans, Louisiana, USA, 2012.

[34] P. Anglin; S. J. Reeves and B. S. Thurow, "Efficient volumetric estimation from plenoptic data," 2013, pp. 90200T-90200T-11.

[35] M. Greene and V. Sick, "Volume-resolved flame chemiluminescence and laser-induced fluorescence imaging," Applied Physics B, vol. 113, pp. 87-92, 2013/10/01 2013.

[36] H. Nien; J. A. Fessler and V. Sick, "Model-based image reconstruction of chemiluminescence using a plenoptic 2.0 camera," presented at the ICIP 2015 IEEE International Conference on Image Processing, Québec City, Canada, 2015.

[37] P. M. Lillo; M. L. Greene and V. Sick, "Plenoptic single-shot 3D imaging of in-cylinder fuel spray geometry," Zeitschrift für Physikalische Chemie, vol. 229, pp. 549 – 560, 2015.

[38] H. Chen; P. M. Lillo and V. Sick, "Three-dimensional spray–flow interaction in a spark-ignition direct-injection engine," International Journal of Engine Research, vol. 17, pp. 129 – 138, January 1, 2016.

[39] W. F. Timothy; P. L. Kyle and S. T. Brian, „Volumetric particle image velocimetry with a single plenoptic camera," Measurement Science and Technology, vol. 26, p. 115201, 2015.

[40] K. Lynch, "Development of a 3-D Fluid Velocimetry Technique based on Light Field Imaging," Master of Science, Aerospace Engineering, Auburn university, 2011.

[41] K. P. Lynch and B. S. Thurow, "Preliminary Development of a 3-D, 3-C PIV Technique using Light Field Imaging," presented at the 41st AIAA Fluid Dynamics Conference and Exhibit, Honolulu, Hawaii, 2011.

[42] B. S. Thurow and T. Fahringer, „Recent Development of Volumetric PIV with a Plenoptic Camera," presented at the 10th International Symposium on Particle Image Velocimetry – PIV13, Delft, The Netherlands, 2013.

[43] C. Perwaß and L. Wietzke, "Single lens 3D-camera with extended depth-of-field," in Human Vision and Electronic Imaging XVII, Burlingame, California, USA, 2012, p. 829108

[44] B. Peterson and V. Sick, "Simultaneous flow field and fuel concentration imaging at 4.8 kHz in an operating engine," Applied Physics B, vol. 97, pp. 887-895, 2009.

[45] P. Schiffmann; S. Gupta; D. Reuss; V. Sick, X. Yang and T.-W. Kuo, "TCCIII - Engine Benchmark for Large Eddy Simulation of IC Engine Flows," Oil & Gas Science and Technology, vol. 71, p. 3, 2016.

[46] H. Bensler; C. Freek; B. Beesten; A. Ritter and A. W. Hentschel, "An Experimental and Numerical Study of the Steady-State Flow of a SI-Engine Intake Port," in SAE Technical Paper 982470, 1998.

[47] H. Bensler; L. Kapitza; J. Raposo and U. Reisch, "A New Experimental Method for Determining Port Generated Swirl Flow," in SAE Technical Paper 2002-01-2846, 2002.

[48] R. D. Keane and R. J. Adrian, "Optimization of particle image velocimeters. Part I: Double pulsed systems," Measurement Science and Technology, vol. 1, pp. 1202 – 1215, 1990.

[49] M. Megerle; V. Sick and D. L. Reuss, "Measurement of Digital PIV Precision using Electrooptically-Created Particle-Image Displacements," Measurement Science and Technology, vol. 13, pp. 997 – 1005, 2002.